

Mechanism of Interfacial Reactions Between Type 430 Stainless Steel and Complex MgO–Al₂O₃–SiO₂–CaO–MnO Oxide During Isothermal Heating



WENLIANG GAN, CHENGSONG LIU, KAI LIAO, HUA ZHANG, and HONGWEI NI

To quantitatively study the mechanism of interfacial reactions between type 430 stainless steel and complex MgO–Al₂O₃–SiO₂–CaO–MnO oxide during the soaking process before hot-rolling, diffusion couple experiments at 1373 K and 1673 K (1100 °C and 1400 °C) with different MnO and SiO₂ contents were conducted. Experimental results showed that the “solid–liquid” and “solid–solid” steel–oxide reactions occurred between the Cr, Mn and Si in the steel and the MnO and SiO₂ in the MgO–Al₂O₃–SiO₂–CaO–MnO oxide during the heating at 1373 K and 1673 K (1100 °C and 1400 °C), respectively, resulting in a change of steel and oxide compositions. Calculations on the Gibbs free energy changes of those steel–oxide reactions before and after isothermal heating indicated the thermodynamic equilibrium at the interface of the steel and oxide were generally achieved after the heating at 1373 K and 1673 K (1100 °C and 1400 °C) for 240 min. Diffusion coefficients of related elements in type 430 stainless steel at 1373 K and 1673 K (1100 °C and 1400 °C) were calculated: Cr, Mn, and Si at 1673 K (1400 °C) are in the range of 1.44 to 3.40 × 10⁻¹², 0.42 to 1.19 × 10⁻¹¹ and 0.52 to 1.34 × 10⁻¹¹ m² m⁻¹, respectively, while Mn and Si at 1373 K (1100 °C) are in the range of 0.80 to 3.71 × 10⁻¹³ and 1.04 to 5.64 × 10⁻¹³ m² s⁻¹, respectively.

<https://doi.org/10.1007/s11663-022-02551-0>

© The Minerals, Metals & Materials Society and ASM International 2022

I. INTRODUCTION

STAINLESS steel grade 430 is a type of non-hardenable stainless steel with ferrite-dominated microstructure at room temperature. Compared with austenitic stainless steel, ferrite stainless steel has the advantages of lower cost, higher mechanical strength and forming properties, better chloride stress corrosion resistance, high temperature oxidation resistance, and thermal conductivity.^[1–5] It is widely used in the fields of household appliance, structural application,^[6] fuel cell,^[7] automotive exhaust system,^[2] power plant condenser^[8] and soft magnetic material.^[9]

Previous studies^[10–17] have proved that non-metallic inclusions in the as-cast steel could transform during isothermal heating before hot rolling. It means that the final inclusions in the steel products are usually not the same as those in the as-cast steel, which may significantly affect the properties of steel products.^[18] Wang *et al.*^[19] investigated the evolution of inclusions in EH36 shipbuilding steel during heating at 1473 K (1200 °C) by SEM and CLSM. It was found that fine TiN inclusions precipitated massively in the steel during the heating, which inhibited the growth of austenite grain. Yang *et al.*^[20] studied the effects of heating temperature, holding time and cooling mode on the inclusion evolution in Ti–Zr deoxidized low carbon steel. During heating in the range of 1100 °C to 1400 °C (1373 K to 1673 K) for 2 hours, the shape of the Ti–Zr oxide changed from an irregular, curved surface to a smooth and spherical surface and the composition distribution of Ti–Zr oxide changed from homogeneous to heterogeneous. Zaitsev *et al.*^[21] experimentally proved that the corrosion activity of oxide-sulfide inclusions decreased with increasing heating temperature and time, leading to the enhancement of local corrosion resistance of the structural steel. Zhang *et al.*^[22] reported that CaO–SiO₂–Al₂O₃–MgO inclusions in as-cast heavy rail steel partly transformed to CaS–MgO·Al₂O₃ during heating in the range of 1000 °C to 1300 °C (1273 to 1573 K), which were quite rigid and harmful to the performance

WENLIANG GAN, CHENGSONG LIU, HUA ZHANG, and HONGWEI NI are with the The State Key Laboratory of Refractories and Metallurgy, Wuhan University of Science and Technology, Wuhan 430081, P.R. China and with the Hubei Provincial Key Laboratory for New Processes of Ironmaking and Steelmaking, Wuhan University of Science and Technology, Wuhan 430081, P.R. China. Contact e-mails: liuchengsong@wust.edu.cn; nihongwei@wust.edu.cn KAI LIAO is with the Huangshi Product Quality Supervision and Inspection Institute, Huangshi 435000, P.R. China.

Manuscript submitted February 22, 2022; accepted May 5, 2022.

Article published online May 16, 2022.

of steel rails. Guo *et al.*^[23] investigated the evolution mechanism of MnO–Al₂O₃–SiO₂ based inclusions during isothermal heating at 1523 K (1250 °C) in 18 wt pct Cr–8wt pct Ni stainless steel. Due to the interfacial reactions between the steel and the inclusions and the Ostwald ripening effect, the plasticity of inclusions decreased. In our previous work,^[24] isothermal heating experiments at 1473 K (1200 °C) were conducted to investigate the thermodynamic mechanisms of inclusion transformation in type 430 stainless steel. The interfacial reactions between the steel matrix and MgO–Al₂O₃–SiO₂–CaO inclusions resulted in an increase in the content of Al₂O₃–TiO_x–Cr₂O₃–MnO spinel in the inclusion. However, under different heat treatment temperatures, those inclusions present in either solid or liquid state. Effect of oxide composition on the “solid–liquid” and “solid–solid” steel–oxide interface reactions at high temperature in type 430 stainless steel and its quantitative analysis are still unknown, which is essential for subsequent hot rolling processes and the steel quality control.

In this work, to precisely control the physicochemical characteristics of inclusions and inhibit their adverse effects on the steel properties, diffusion couple experiments at 1373 K and 1673 K (1100 °C and 1400 °C) between type 430 stainless steel and the complex MgO–Al₂O₃–SiO₂–CaO–MnO oxide with different MnO and SiO₂ contents were conducted to quantitatively study the mechanism of “solid–liquid” and “solid–solid” steel–oxide interface reactions during the soaking process before hot-rolling. The morphologies of steel–oxide interfaces and chemical compositions of typical phases in the diffusion couple samples were measured and analyzed. Thermodynamic equilibrium calculations between the type 430 stainless steel and the complex MgO–Al₂O₃–SiO₂–CaO–MnO oxide at 1373 K and 1673 K (1100 °C and 1400 °C) were performed. Finally, the diffusion coefficients of Cr, Mn, Si elements in type 430 stainless steel at 1373 K and 1673 K (1100 °C and 1400 °C) were obtained.

II. EXPERIMENTAL METHOD

A. Diffusion Couple Experiment

The chemical composition of type 430 stainless steel for the diffusion couple experiments at 1373 K and 1673 K (1100 °C and 1400 °C) was determined by inductively coupled plasma mass spectrometry (ICP–MS), combustion analysis (for S) and nitrogen/oxygen analysis (for N and O). The results are listed in Table I.

The as-cast 430 stainless steel was machined into an approximate cylinder ($\Phi 5 \times 3$ mm), containing a small circular hole ($\Phi 3$ mm) to place the complex MgO–Al₂O₃–SiO₂–CaO–MnO oxide powder. Effects of MnO and SiO₂ contents in the oxide on the steel–oxide interfacial reactions were studied, separately. The chemical compositions of the complex oxides are listed in Table II. Here, the codes A, B, C and D refer to the complex oxides with 0, 5, 10, 15 pct MnO content respectively (mass pct), where the mass ratios of other

components remain constant. The chemical composition of oxide B was set as a standard, and the codes E, F, G, and H refer to the complex oxides with 37.15, 45.41, 49.54, and 53.66 pct SiO₂ content respectively.

To prepare the complex oxide, MgO, Al₂O₃, SiO₂, CaO and MnO powders with high purity (≥ 99.9 pct) were mixed. Through thermogravimetry and differential thermal analysis (TG-DTA), the melting points of those complex oxides were measured and are also shown in Table II; all of them are below 1610 K (1337 °C). The mixture was pre-melted at 1923 K (1650 °C) in a tube furnace and quenched in ice water immediately after holding for 45 min. A platinum crucible was used for oxide pre-melting to avoid oxide composition variation caused by interfacial reactions with oxide crucible. A homogeneous glassy complex MgO–Al₂O₃–SiO₂–CaO–MnO oxide was obtained due to the high cooling rate. After grinding, it (~15 mg) was placed into the small circular hole on the steel sample. A confocal scanning laser microscope (CSLM; VL2000DX-SVF17SP, Lasertec Corporation, Japan) was employed to bond the steel and the complex oxide. Before bonding, the CSLM chamber was vacuumed to 5.0×10^{-3} Pa and purged with high purity Ar gas (99.9 pct) 3 times to inhibit oxidation at high temperature. To obtain good contact, the bonding temperature was 50 K above the melting temperature of each complex oxide and the heating rate was 200 K/min. As soon as the oxide melted, the diffusion couples were quenched with helium gas immediately. Figure 1(a) shows the experimental set-up for bonding in CSLM.

The prepared diffusion couple was then sealed in a quartz tube which was first evacuated to approximately 5×10^{-3} Pa, and then filled with high purity Ar gas (99.9 pct) to approximately 2×10^4 Pa. A Ti foil was introduced into the quartz tube to further lower the oxygen partial pressure and protect the diffusion couple against oxidation during subsequent isothermal heating. A type 430 stainless steel block was placed between the diffusion couple sample and the Ti foil to prevent contamination. The quartz tube was subjected to isothermal heating experiments at 1373 K and 1673 K (1100 °C and 1400 °C) using a muffle furnace; the holding time was 240 min. To maintain the original state of the diffusion couple at high temperature, the quartz tube was water-quenched immediately after isothermal heating. The diffusion couple A after bonding in CSLM and isothermal heating at 1373 and 1673 K (1100 °C and 1400 °C) were named as A-0, A-1100 and A-1400, respectively, and so on for each of other 7 diffusion couples. Figure 1(b) shows the temperature curves for the full experimental procedure.

B. Specimen Analysis

After isothermal heating, the specimens were ground with SiC abrasive paper and polished with diamond polishing paste. The morphologies of the steel–oxide interfaces and chemical compositions of typical phases in the diffusion couple samples were measured by scanning electron microscopy (SEM) and energy-dispersive spectroscopy (EDS) (Apreo S HiVac, Thermo

Table I. Chemical Composition of the Type 430 Stainless Steel Used in the Diffusion Couple Experiments

Element	Cr	Ni	C	Si	Mn	P	S	Al	Ti	N	O
Content/Mass Pct	16.2	0.13	0.035	0.3	0.33	0.02	0.002	0.001	<0.001	0.036	0.003

Table II. Chemical Compositions of the Complex MgO–Al₂O₃–SiO₂–CaO–MnO Oxides Used in the Diffusion Couple Experiments

Oxide No.	MgO	Al ₂ O ₃	SiO ₂	CaO	MnO	Melting Point/K
(A) Oxide—0 Pct MnO	12.21	15.15	43.45	29.19	0	1560 (1287 °C)
(B) Oxide—5 Pct MnO (41.28 Pct SiO ₂)	11.60	14.39	41.28	27.73	5.00	1552 (1279 °C)
(C) Oxide—10 Pct MnO	10.99	13.64	39.11	26.27	10.00	1537 (1264 °C)
(D) Oxide—15 Pct MnO	10.38	12.88	36.93	24.81	15.00	1532 (1259 °C)
(E) Oxide—37.15 Pct SiO ₂	12.42	15.40	37.15	29.68	5.35	1606 (1333 °C)
(F) Oxide—45.41 Pct SiO ₂	10.78	13.38	45.41	25.78	4.65	1516 (1243 °C)
(G) Oxide—49.54 Pct SiO ₂	9.97	12.37	49.54	23.83	4.30	1528 (1255 °C)
(H) Oxide—53.66 Pct SiO ₂	9.15	11.36	53.66	21.88	3.95	1528 (1255 °C)

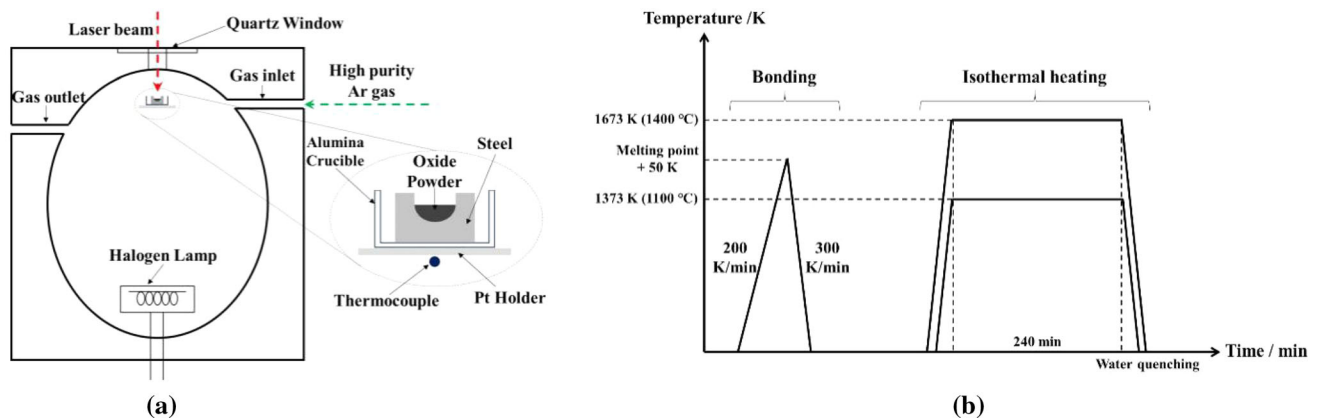


Fig. 1—(a) Experimental set-up for bonding in CSLM and (b) temperature curves for the full experiment procedure.

Fisher Scientific Inc., USA). The chemical compositions of steel and oxide near the steel–oxide interface were analyzed using an electron probe microanalyzer (EPMA, 8050G, Shimadzu, Japan) operated at an accelerating voltage of 15 kV and a beam current of 100 nA. The peak intensities of elements in the steel and complex oxides were calibrated against standard samples to reduce measurement errors.

III. RESULTS

A. Morphology and Element Distributions at the Interface Between the Steel and the Oxide

Figure 2 shows the SEM images of steel–oxide interface in the diffusion couples with different MnO and SiO₂ contents in the oxides after bonding. The chemical compositions of different phases in the complex MgO–Al₂O₃–SiO₂–CaO–MnO oxide shown in Figure 2 are listed in Table III. Good contact was obtained between the steel and the complex oxide after bonding, as evidenced by Figure 2. All oxides presented an almost homogeneous state due to the high cooling

rate in CSLM. The chemical compositions of those complex oxides prepared for subsequent isothermal heating were very close to the initial pre-melted mixtures, as shown in Table II. The valence of chromium oxide at different temperatures will be discussed in Section IV later.

Figure 3 shows the SEM images of the steel–oxide interface in the diffusion couples with different MnO and SiO₂ contents in the oxides after isothermal heating at 1673 K (1400 °C) for 240 min. The chemical compositions of different phases in the complex MgO–Al₂O₃–SiO₂–CaO–MnO oxides shown in Figure 3 are listed in Table IV. The oxides were in an almost homogeneous state since the specimens were water-quenched after isothermal heating at 1673 K (1400 °C). The chemical compositions of complex oxides in all cases varied significantly due to the “solid–liquid” steel–oxide reaction during heating at 1673 K (1400 °C), since the melting points of oxides in all cases were lower than 1673 K (1400 °C). The chromium oxide content generally increased with the increase of MnO and SiO₂ contents, while the variation amplitudes of MnO and SiO₂ contents depended on their initial contents.

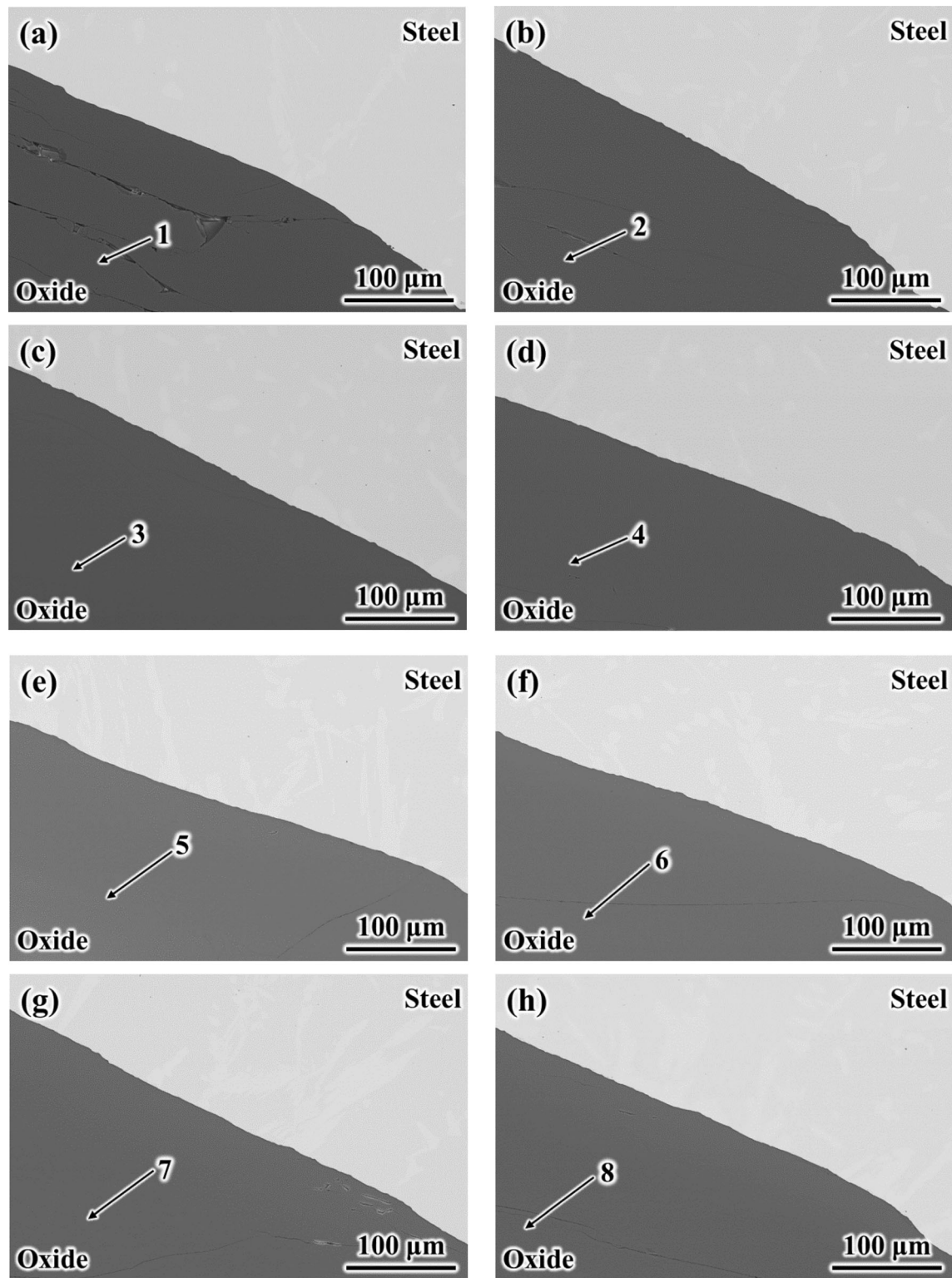


Fig. 2—SEM images of the steel–oxide interface in the diffusion couples: (a) A-0 (b) B-0, (c) C-0, (d) D-0, (e) E-0 (f) F-0, (g) G-0, and (h) H-0.

Figure 4 shows the SEM images of the steel–oxide interface in the diffusion couples with different MnO and SiO₂ contents in the oxides after isothermal heating at 1373 K (1100 °C) for 240 min. The chemical compositions of different phases in the complex MgO–Al₂O₃–SiO₂–CaO–MnO oxides shown in Figure 4

are listed in Table V. After heating at 1373 K (1100 °C), some grey phases with relatively higher brightness were observed in the bulk oxides (Figures 4(a) through (f)), except for the diffusion couples with higher SiO₂ contents in the oxides (Figures 4(g) and (h)). Compared with the dark phases, the grey phases contained higher

Table III. Chemical Compositions of Different Phases in the Complex MgO–Al₂O₃–SiO₂–CaO–MnO Oxide Shown in Fig. 2

Oxide/Mass Pct	MgO	Al ₂ O ₃	SiO ₂	CaO	CrO	MnO
Point 1	11.45	15.54	44.70	28.10	0.16	0.05
Point 2	11.62	14.33	42.30	26.62	0.49	4.64
Point 3	9.83	14.09	40.23	26.24	0.25	9.37
Point 4	9.37	13.06	38.42	25.14	0.50	13.51
Point 5	11.66	14.40	39.68	28.70	0.36	5.21
Point 6	10.24	13.20	47.16	24.70	0.20	4.51
Point 7	9.67	12.53	50.81	22.73	0.16	4.10
Point 8	8.89	11.78	54.31	21.05	0.19	3.77

CaO and MnO contents but lower Al₂O₃ content (Points 5 and 7 listed in Table V). With the increase of initial MnO content in the complex oxide, the grey phases transformed from Ca-rich CaO–SiO₂–MgO–Al₂O₃–MnO oxides to Mn-rich CaO–MnO–SiO₂–MgO oxides with almost no Al₂O₃. With the increase of initial SiO₂ content in the complex oxide, the grey phases gradually disappeared, as shown in Figures 4(g) and (h). In addition, interfacial reaction layers in the oxides near the steel–oxide interfaces were observed due to the “solid–solid” steel–oxide reaction during heating at 1373 K (1100 °C).

Figure 5 shows the mapping analysis results of Cr, Mn, Si, Ca, Mg, Al, Fe and O in the steel and oxide near the interface in the diffusion couple D (Oxide—15 pct MnO) after isothermal heating at 1673 K (1400 °C) and 1373 K (1100 °C) for 240 min. After isothermal heating at 1673 K (1400 °C), no reaction layer or concentration gradient in the steel and oxide were observed near the interface, as shown in Figure 5(a). The distributions of all elements in the complex oxide were almost homogeneous, which indicated that the oxide was all in liquid state at 1673 K (1400 °C). Due to the “solid–liquid” steel–oxide reaction during heating at 1673 K (1400 °C), Cr content in the oxide increased significantly. After isothermal heating at 1373 K (1100 °C), phase separation could be observed in the oxide, as shown in Figure 5(b). Reaction layers both in the oxide and steel near the interface after heating at 1373 K (1100 °C) were found. As indicated by numbers 1 and 2 in Figure 5(b), the CrO content in the oxide reaction layer was relatively higher than that in the bulk oxide, while the Cr content in the steel reaction layer was lower than that in the bulk steel.

Figure 6 shows the mapping analysis results of Cr, Mn, Si, Ca, Mg, Al, Fe and O in the steel and oxide near the interface in the diffusion couple F (Oxide—45.41 pct SiO₂) after isothermal heating at 1673 K (1400 °C) and 1373 K (1100 °C) for 240 min. Results were generally similar to those shown in Figure 5. There was no reaction layer or concentration gradient observed in the steel and oxide near the interface after isothermal heating at 1673 K (1400 °C), and phase separation could also be observed in the oxide after isothermal heating at 1373 K (1100 °C). However, the grey phases shown in Figure 6(b) were Ca-rich CaO–SiO₂–Al₂O₃–MgO–MnO oxides, while those in Figure 5(b) were Mn-rich CaO–MnO–SiO₂–MgO oxides. As

indicated by numbers 1 to 4 in Figure 6(b), the Cr, Mn content in the steel and CrO, MnO content in the oxide near the interface varied significantly due to the “solid–solid” steel–oxide reaction during heating at 1373 K (1100 °C).

B. Changes in the Chemical Compositions of the Steel and Oxide Near the Interface

In our previous study,^[24] the CaO, Al₂O₃, and MgO content in the complex inclusions generally remained stable after the interface reaction between the steel and inclusions during heating. Similar results were also obtained in this study for diffusion couple experiments at 1373 K and 1673 K (1100 °C and 1400 °C). Thus, only elements Cr, Mn and Si in the steel and complex oxide are shown and discussed in this section. Figure 7 shows the changes of Cr, Mn and Si content in the steel and CrO, MnO and SiO₂ in the complex oxide for diffusion couples A, B, C and D near the steel–oxide interface after isothermal heating at 1673 K (1400 °C) for 240 min. In Figures 7 through 11, the dash lines with different colors indicate the initial contents of elements or oxide components in different cases before heating.

As shown in Figures 7(a) through (c), after isothermal heating at 1673 K (1400 °C), there were significant concentration gradients of Cr, Mn and Si in the steel near the steel–oxide interface. As the initial MnO content in the complex oxide increased from 0 to 15 mass pct, the Cr content in the steels in all cases decreased slightly (from an initial value of 16.2 mass pct to approximately 15.6 to 15.9 mass pct at the interfaces) while the Mn and Si contents varied depending on the initial MnO contents in the complex oxide. Mn content at the interface of diffusion couples A-1400, B-1400, C-1400 and D-1400 changed from an initial value of 0.33 mass pct to approximate 0.237, 0.318, 0.369 and 0.471 mass pct, respectively. Si content at a distance of 50 μm changed from an initial value of 0.3 mass pct to approximately 0.341, 0.337, 0.218 and 0.203 mass pct in the diffusion couple A-1400, B-1400, C-1400 and D-1400, respectively, while in all cases, the Si content in the steel decreased sharply within 50 μm distance from the interface. This phenomenon will be discussed in Section IV later.

After isothermal heating at 1673 K (1400 °C), all complex oxides presented an almost homogeneous state with hardly no concentration gradient. As the initial MnO content in the complex oxide increased from 0 to 15 pct, the average CrO content in the oxide increased from an initial value of 0 mass pct to approximately 2.75, 2.95, 3.14 and 3.53 mass pct in the diffusion couples A-1400, B-1400, C-1400 and D-1400 after heating, respectively. The average MnO content in the oxide changed from 0 (A-1400), 5 (B-1400), 10 (C-1400) and 15 mass pct (D-1400) initially to approximately 2.34, 4.08, 5.09 and 7.08 mass pct, respectively, and the average SiO₂ content in the oxide changed from 43.45 (A-1400), 41.28 (B-1400), 39.11 (C-1400) and 36.93 mass pct (D-1400) initially to approximately 42.04, 41.93, 41.06 and 40.81 mass pct, respectively, as shown in Figures 7(d) through (f).

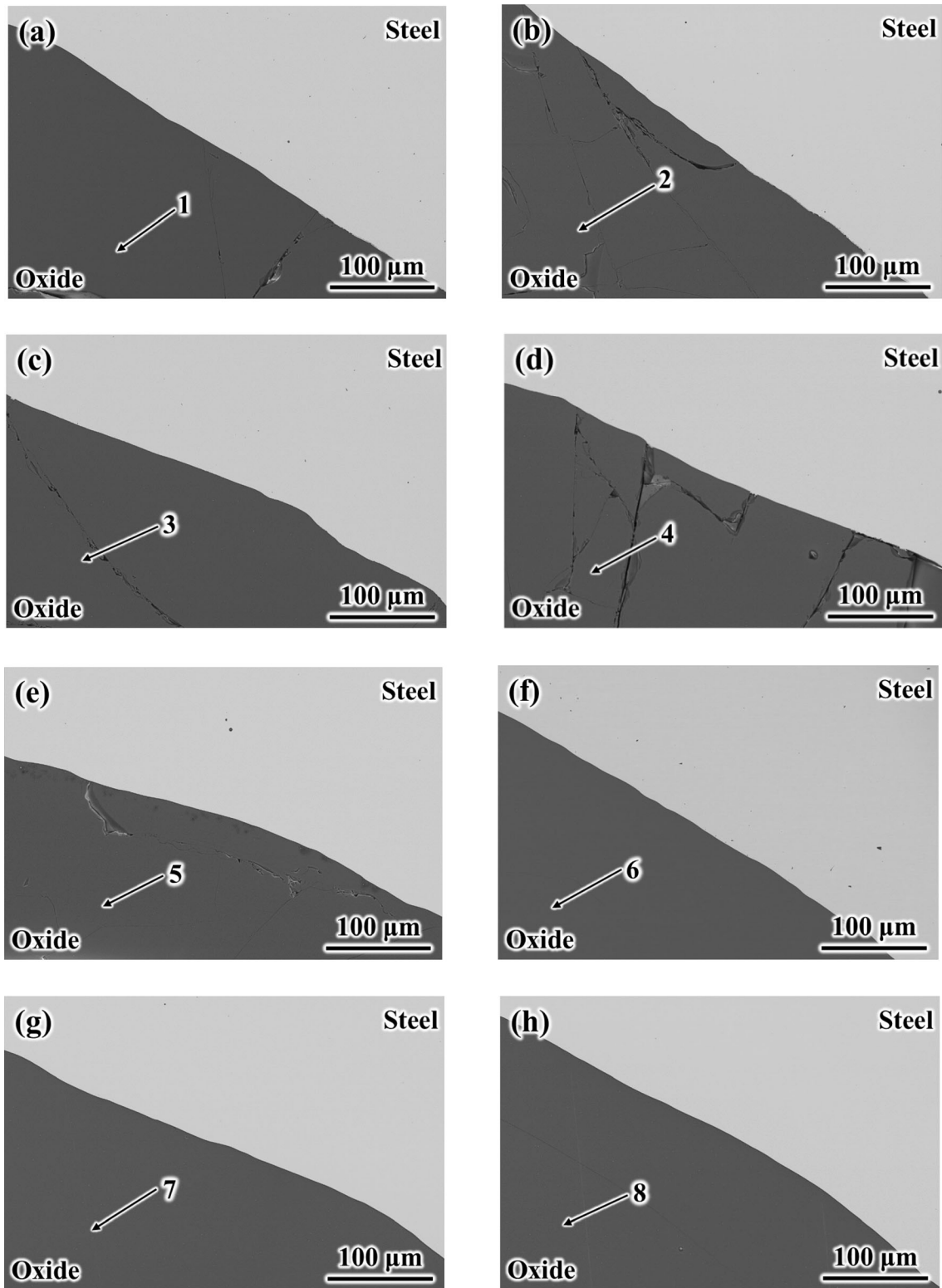


Fig. 3—SEM images of the steel–oxide interface in the diffusion couples: (a) A-1400 (b) B-1400, (c) C-1400, (d) D-1400, (e) E-1400 (f) F-1400, (g) G-1400, and (h) H-1400.

Figure 8 shows the changes of Cr, Mn and Si content in the steel and CrO, MnO and SiO₂ content in the complex oxide of diffusion couples E, B, F, G and H near the steel–oxide interface after isothermal heating at 1673 K (1400 °C) for 240 min.

Concentration gradients of Cr, Mn and Si in the steel, the sharp decrease of Si content near the interface and homogeneous complex oxides with no concentration gradients were also observed after heating, which were similar to Figure 7.

Table IV. Chemical Compositions of Different Phases in the Complex MgO–Al₂O₃–SiO₂–CaO–MnO Oxide Shown in Fig. 3

Oxide/Mass Pct	MgO	Al ₂ O ₃	SiO ₂	CaO	CrO	MnO
Point 1	11.98	14.44	41.34	26.22	3.29	2.73
Point 2	10.88	15.11	40.79	24.99	3.74	4.48
Point 3	10.23	14.53	40.90	25.08	3.97	5.29
Point 4	10.40	13.79	40.55	23.42	4.36	7.48
Point 5	11.48	15.49	39.32	27.17	2.87	3.67
Point 6	11.02	13.68	43.14	22.41	4.92	4.82
Point 7	9.76	11.93	46.24	22.10	5.50	5.47
Point 8	8.22	11.45	48.51	18.60	7.16	6.07

As shown in Figures 8(a) through (c), as the initial SiO₂ content in the complex oxide increased from 37.15 to 53.66 mass pct, the Cr content in the steels in all cases decreased slightly (from an initial value of 16.2 mass pct to approximately 15.6 to 15.9 mass pct at the interface) while the Mn and Si content varied also depending on the initial SiO₂ contents in the complex oxide. Mn content at the interface of diffusion couples E-1400, B-1400, F-1400, G-1400 and H-1400 changed from an initial value of 0.33 mass pct to approximately 0.369, 0.318, 0.303, 0.286 and 0.242 mass pct, respectively. Si content at the distance of 50 μm changed from an initial value of 0.3 mass pct to approximately 0.224, 0.320, 0.378, 0.396 and 0.452 mass pct in the diffusion couples E-1400, B-1400, F-1400, G-1400 and H-1400, respectively.

As the initial SiO₂ content in the complex oxide increased from 37.15 to 53.66 mass pct, the average CrO content in the oxide increased from an initial value of 0 mass pct to approximately 2.46, 2.95, 3.85, 4.87 and 6.05 mass pct in the diffusion couple E-1400, B-1400, F-1400, G-1400 and H-1400, respectively. The average MnO content in the oxide changed from 5.35 (E-1400), 5.00 (B-1400), 4.65 (F-1400) 4.30 (G-1400) and 3.95 mass pct (H-1400) initially to approximately 3.36, 4.08, 4.68, 5.23 and 5.63 mass pct, respectively, and the average SiO₂ content in the oxide changed from 37.15 (E-1400), 41.28 (B-1400), 45.41 (F-1400) 49.54 (G-1400) and 53.66 mass pct (H-1400) initially to approximately 39.12, 41.93, 42.31, 46.53 and 47.88 mass pct, respectively, as shown in Figures 8(d) through (f).

Figure 9 shows the changes of Cr, Mn and Si contents in the steel and Cr₂O₃, MnO and SiO₂ content in the complex oxide of diffusion couples A, B, C and D near the steel–oxide interface after isothermal heating at 1373 K (1100 °C) for 240 min. The bulk steel was separated into two phases with approximate 15 and 17 mass pct Cr content, respectively, while there was no significant difference of Mn and Si content between the two phases, as shown in Figures 9(a) through (c).

After isothermal heating at 1373 K (1100 °C), there were also significant concentration gradients of Cr, Mn and Si in the steel near the steel–oxide interface. As the initial MnO content in the complex oxide increased from 0 to 15 mass pct, the Cr content in the steel at the interface decreased from 16.2 mass pct initially to

approximately 15.02 (A-1100), 14.72 (B-1100), 14.67 (C-1100) and 14.26 mass pct (D-1100). The Mn content in the steel at the interface changed from 0.33 mass pct initially to approximately 0.262 (A-1100), 1.057 (B-1100), 1.261 (C-1100) and 1.704 mass pct (D-1100). The Si content in the steel at the interface changed from 0.3 mass pct initially to approximately 0.434 (A-1100), 0.376 (B-1100), 0.297 (C-1100) and 0.262 mass pct (D-1100). The change trends of Cr, Mn and Si contents in the steel near the interface were similar to the results after heating at 1673 K (1400 °C), while the diffusion widths of them were all less than 150 μm, as shown in Figures 9(a) through (c).

After heating at 1373 K (1100 °C), there were significant phase separations in the complex oxides in diffusion couples A-1100, B-1100, C-1100 and D-1100, whose morphologies and chemical compositions were shown in Figure 4 and Table V. As the initial MnO content in the complex oxide increased from 0 to 15 mass pct, the Cr₂O₃ content at the interface increased from 0 mass pct initially to approximately 1.43 (A-1100), 1.62 (B-1100), 1.70 (C-1100) and 1.88 mass pct (D-1100). The MnO content at the interface changed from 0 (A-1100), 5 (B-1100), 10 (C-1100) and 15 mass pct (D-1100) initially to approximately 0.43, 6.44, 6.25 and 14.42 mass pct, respectively, and the SiO₂ content at the interface changed from 43.45 (A-1100), 41.28 (B-1100), 39.11 (C-1100) and 36.93 mass pct (D-1100) initially to approximately 41.24, 39.59, 40.28 and 37.62 mass pct, as shown in Figures 9(d) through (f).

Figure 10 shows the changes of Cr, Mn and Si content in the steel and Cr₂O₃, MnO and SiO₂ content in the complex oxide of diffusion couples E, B, F, G and H near the steel–oxide interface after isothermal heating at 1373 K (1100 °C) for 240 min.

After isothermal heating at 1373 K (1100 °C), similar concentration gradients of Cr, Mn and Si in the steel near the steel–oxide interface were observed. With the increase of initial SiO₂ content in the oxide from 37.15 to 53.66 mass pct, the Cr content in the steel at the interface decreased from 16.2 mass pct initially to approximately 14.2 mass pct in all cases. The Mn content at the interface changed from 0.33 mass pct initially to approximately 1.384 (E-1100), 1.057 (B-1100), 1.149 (F-1100), 0.709 (G-1100) and 0.322 mass pct (H-1100). The Si content at the interface changed from 0.3 mass pct initially to approximately 0.321 (E-1100), 0.376 (B-1100), 0.397 (F-1100), 0.564 (G-1100) and 0.520 mass pct (H-1100). In the oxide side, the Cr₂O₃ content at the interface increased from 0 mass pct initially to approximately 2.20 (E-1100), 1.62 (B-1100), 1.77 (F-1100), 2.17 (G-1100) and 2.37 mass pct (H-1100). The MnO content at the interface changed from 5.35 (E-1100), 5.00 (B-1100), 4.65 (F-1100), 4.30 (G-1100) and 3.95 mass pct (H-1100) initially to approximately 5.19, 6.44, 3.69, 3.88 and 4.35 mass pct, respectively, and the SiO₂ content at the interface changed from 37.15 (E-1100), 41.28 (B-1100), 45.41 (F-1100) 49.54 (G-1100) and 53.66 mass pct (H-1100) initially to approximately 31.22, 39.59, 41.66, 45.31 and 47.87 mass pct, respectively.

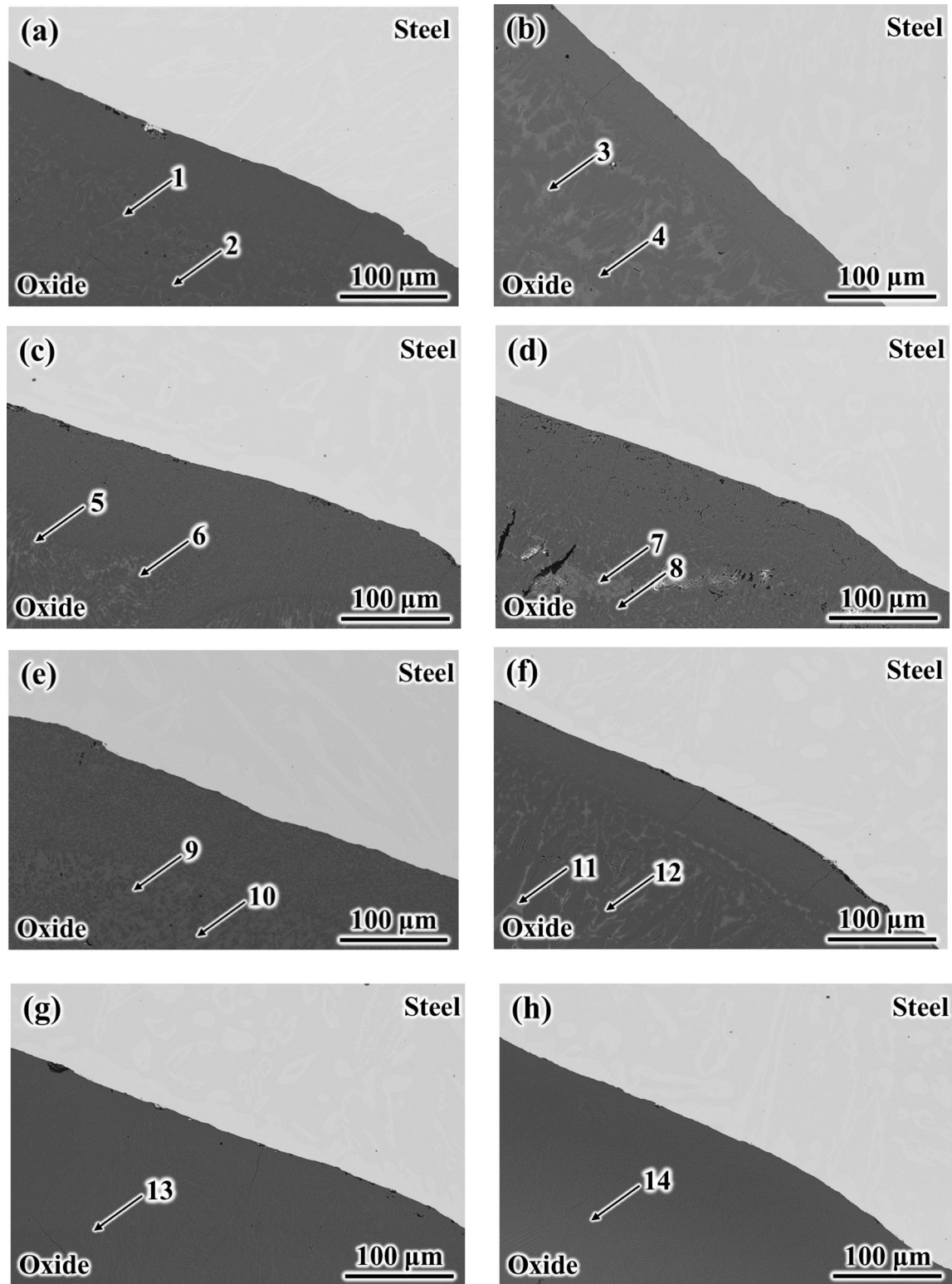


Fig. 4—SEM images of the steel–oxide interface in the diffusion couples: (a) A-1100, (b) B-1100, (c) C-1100 (d) D-1100, (e) E-1100, (f) F-1100, (g) G-1100 and (h) H-1100.

IV. DISCUSSION

A. Thermodynamic Analysis of the Steel–Oxide Interfacial Reaction

In this work, to study the effects of MnO and SiO₂ contents and isothermal heating temperature on the interfacial reaction between type 430 stainless steel and complex MgO–Al₂O₃–SiO₂–CaO–MnO oxide, diffusion couple experiments were conducted at 1673 K (1400 °C) and 1373 K (1100 °C). The “solid–liquid” steel–oxide reaction during heating at 1673 K (1400 °C) and the “solid–solid” steel–oxide reaction during heating at 1373 K (1100 °C) were investigated.

Figures 7 through 10 show that after heating at 1673 K (1400 °C) or 1373 K (1100 °C) for 240 min, the Cr content in the steel near the steel–oxide interface of each diffusion couple decreased significantly. The Mn and Si

Table V. Chemical Compositions of Different Phases in the Complex MgO–Al₂O₃–SiO₂–CaO–MnO Oxide Shown in Fig. 4

Oxide/Mass Pct	MgO	Al ₂ O ₃	SiO ₂	CaO	CrO	MnO
Point 1	9.65	12.50	39.82	38.02	0	0
Point 2	13.86	16.00	44.29	24.63	1.22	0
Point 3	6.28	11.68	38.63	37.33	0	6.07
Point 4	11.94	16.64	42.88	24.63	0.40	3.52
Point 5	11.11	0.37	34.34	28.83	0	25.36
Point 6	9.83	18.90	43.04	24.16	0	4.07
Point 7	12.13	0	34.35	23.08	0	30.44
Point 8	1.95	19.50	37.73	24.92	0	15.90
Point 9	7.54	14.15	36.21	39.52	0	2.59
Point 10	17.25	28.05	33.45	16.86	1.94	2.45
Point 11	1.96	13.48	42.35	28.88	0	13.34
Point 12	11.74	14.79	45.58	23.89	0	4.00
Point 13	9.42	13.06	49.48	22.44	0.53	5.08
Point 14	9.77	12.26	53.30	20.89	0	3.78

contents also changed in varying degrees depending on the initial MnO and SiO₂ content in the oxide, as well as the CrO_x, MnO and SiO₂ content in the oxide. To reveal the mechanism of the steel–oxide interfacial reactions, the precise Cr valence in the chromium oxide during heating were predicted and calculated using the Equilib module of FactSage 8.1 (GTT-Technologies, German). The FToxid database was used for the slag and solid oxide solutions. FactPS was used for the pure substances, and FSstel was used for the solid and liquid steel.

Thermodynamic equilibrium calculations between type 430 stainless steel and the complex oxide B at 1673 K (1400 °C) were performed. Figure 11(a) shows the relationship between the mass ratio of Cr₂O₃ to CrO in the equalized complex oxide B and the mass ratio of the oxide to the steel. Results show that as the mass ratio of the oxide to the steel decreased from 1.0 to 0.001, the mass ratio of Cr₂O₃ to CrO in the equalized complex oxide B only varied in the range of 0.017 to 0.019, which indicated that during isothermal heating at 1673 K (1400 °C), the chromium oxide in the complex oxide should mainly be considered as CrO. The precipitation and transformation of Cr-containing phases which occurred within the complex oxide at different temperatures were also calculated with FactSage 8.1, referring to Figure 11(b). The results show that when the temperature was above 1633 K (1300 °C), mainly CrO oxide existed in the complex liquid oxide. As the temperature decreased, CrO oxide gradually transformed to Cr₂O₃ oxide (mainly in spinel) and Cr (in ferrite). Thus, during isothermal heating at 1373 K (1100 °C), the chromium oxide in the complex oxide should mainly be considered as Cr₂O₃.

Accordingly, the steel–oxide interfacial reactions during isothermal heating at 1673 K (1400 °C) or 1373 K (1100 °C) could be derived by Eqs. [1] through [5]:

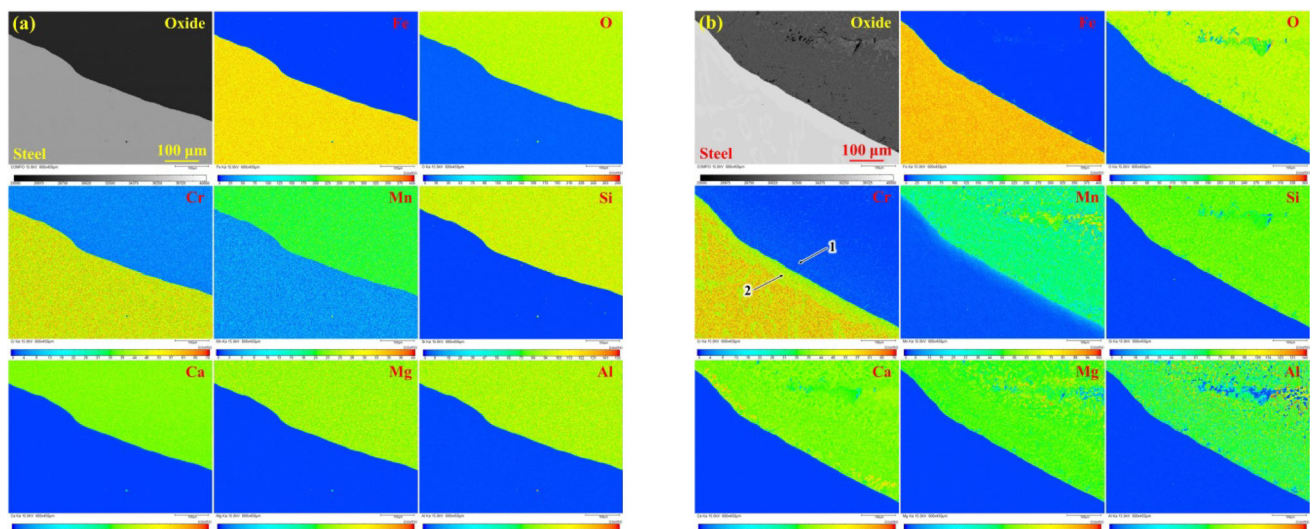


Fig. 5—Measured distributions of Cr, Mn, Si, Ca, Mg, Al, Fe and O in the steel and oxide of diffusion couples: (a) D-1400 and (b) D-1100.

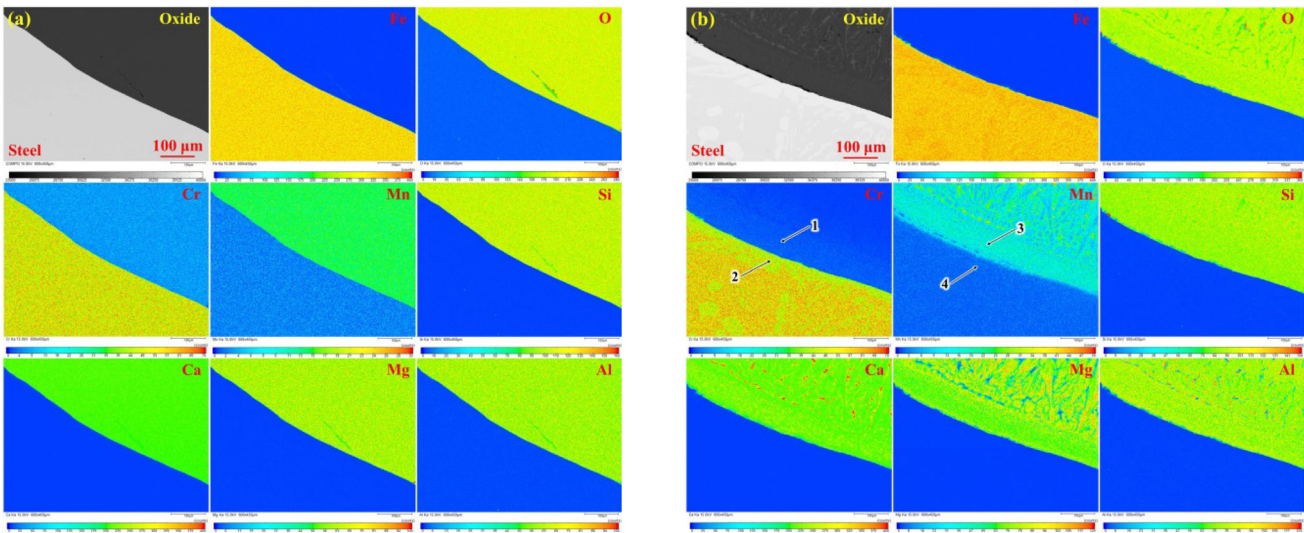


Fig. 6—Measured distributions of Cr, Mn, Si, Ca, Mg, Al, Fe and O in the steel and oxide of diffusion couples (a) F-1400 and (b) F-1100.

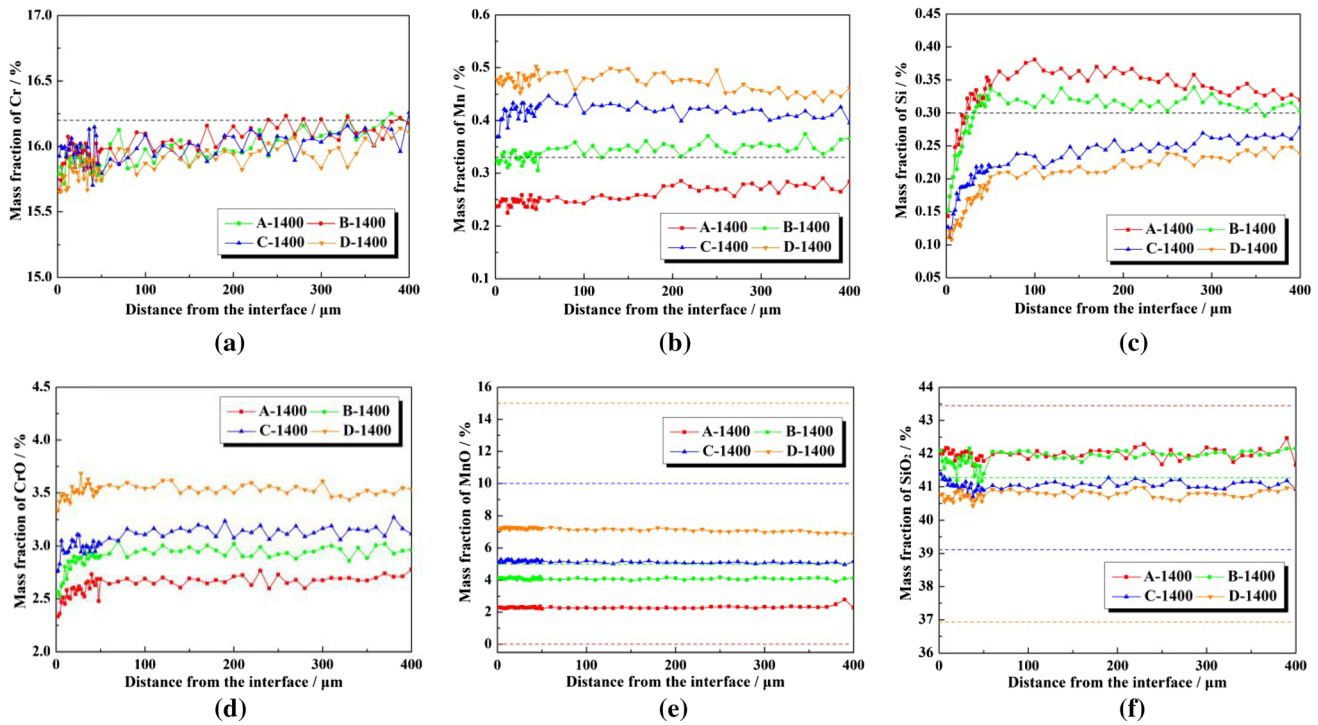
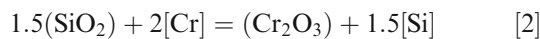


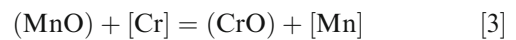
Fig. 7—Changes of (a) Cr, (b) Mn, (c) Si in the steel and (d) CrO, (e) MnO, (f) SiO₂ in the complex oxide of diffusion couples A-1400, B-1400, C-1400, and D-1400 near the steel–oxide interface after isothermal heating at 1673 K (1400 °C) for 240 min.



$$J_1 = \frac{a_{(\text{CrO})}^2 a_{[\text{Si}]}}{a_{[\text{Cr}]}^2 a_{(\text{SiO}_2)}}$$



$$J_2 = \frac{a_{(\text{Cr}_2\text{O}_3)} a_{[\text{Si}]}^{1.5}}{a_{[\text{Cr}]}^2 a_{(\text{SiO}_2)}^{1.5}}$$



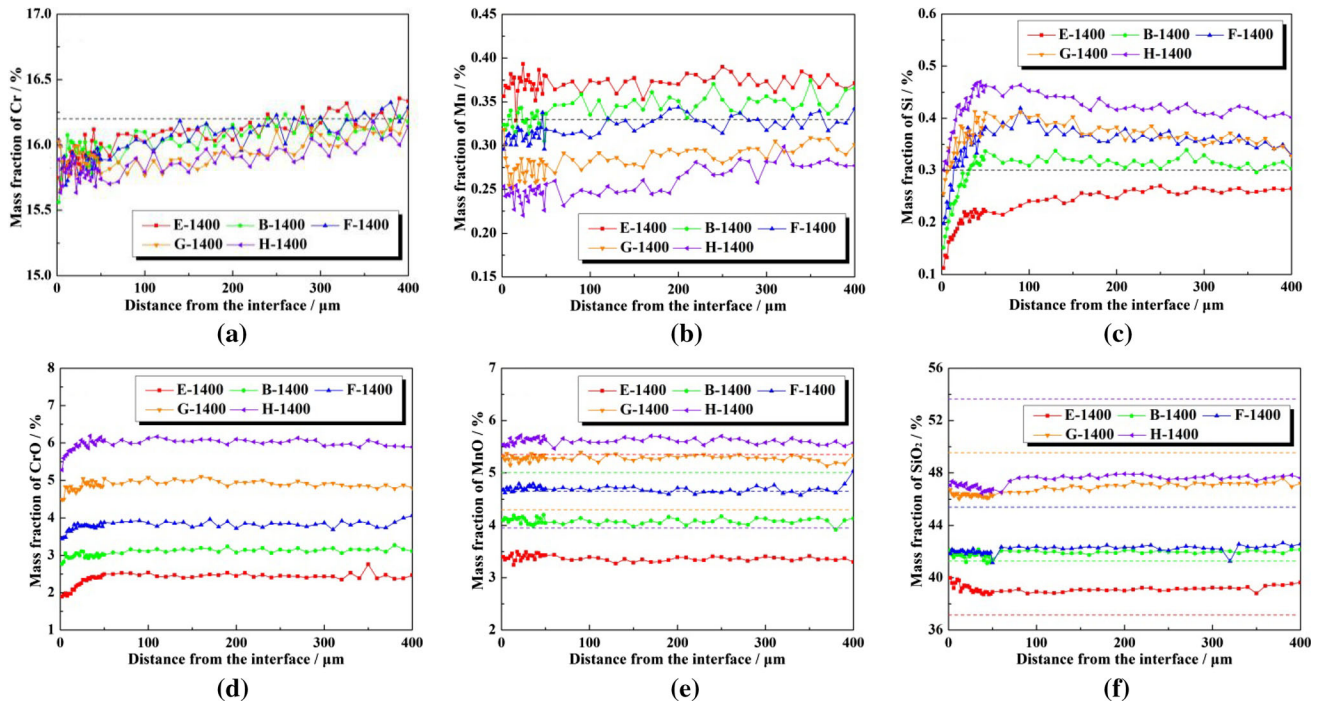


Fig. 8—Changes of (a) Cr, (b) Mn, (c) Si in the steel and (d) CrO, (e) MnO, (f) SiO₂ in the complex oxide of diffusion couples E-1400, B-1400, F-1400, G-1400 and H-1400 near the steel–oxide interface after isothermal heating at 1673 K (1400 °C) for 240 min.

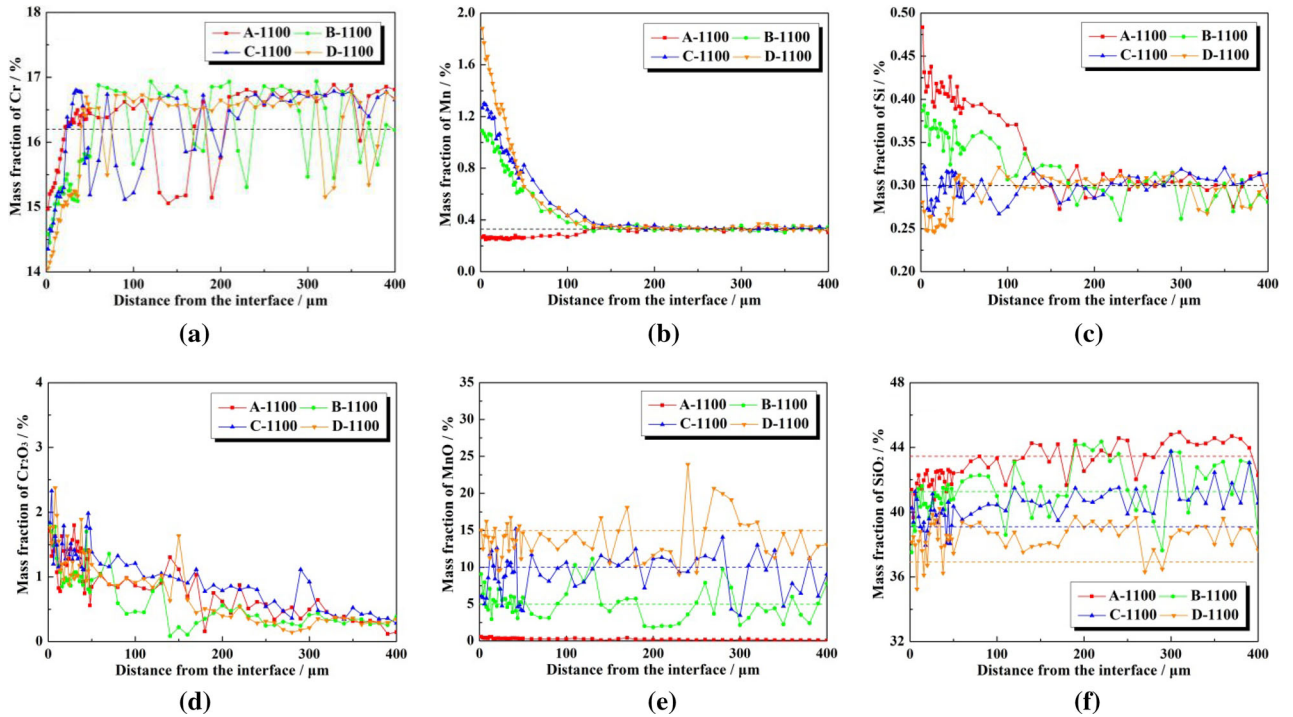


Fig. 9—Changes of (a) Cr, (b) Mn, (c) Si contents in the steel and (d) Cr₂O₃, (e) MnO, (f) SiO₂ in the complex oxide of diffusion couples A-1100, B-1100, C-1100, and D-1100 near the steel–oxide interface after isothermal heating at 1373 K (1100 °C) for 240 min.

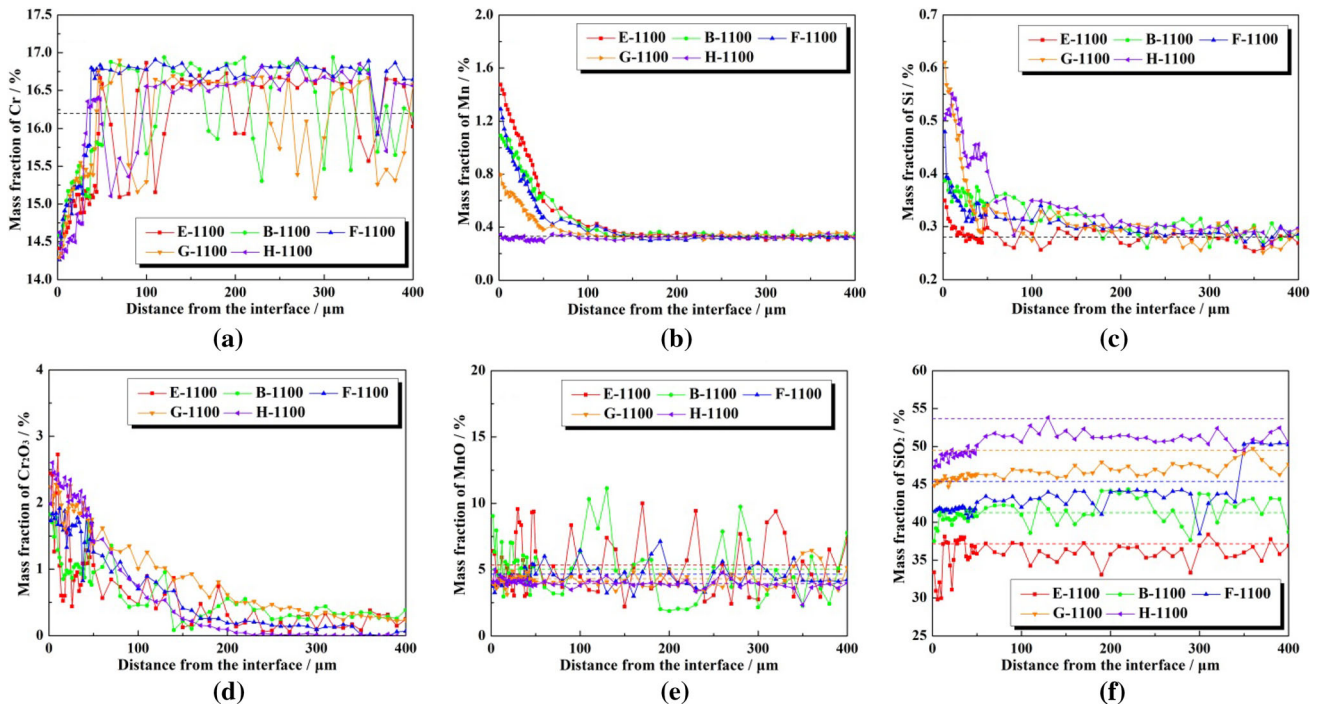


Fig. 10—Changes of (a) Cr, (b) Mn, (c) Si contents in the steel and (d) Cr_2O_3 , (e) MnO, (f) SiO_2 in the complex oxide of diffusion couples E-1100, B-1100, F-1100, G-1100 and H-1100 near the steel–oxide interface after isothermal heating at 1373 K (1100 °C) for 240 min.

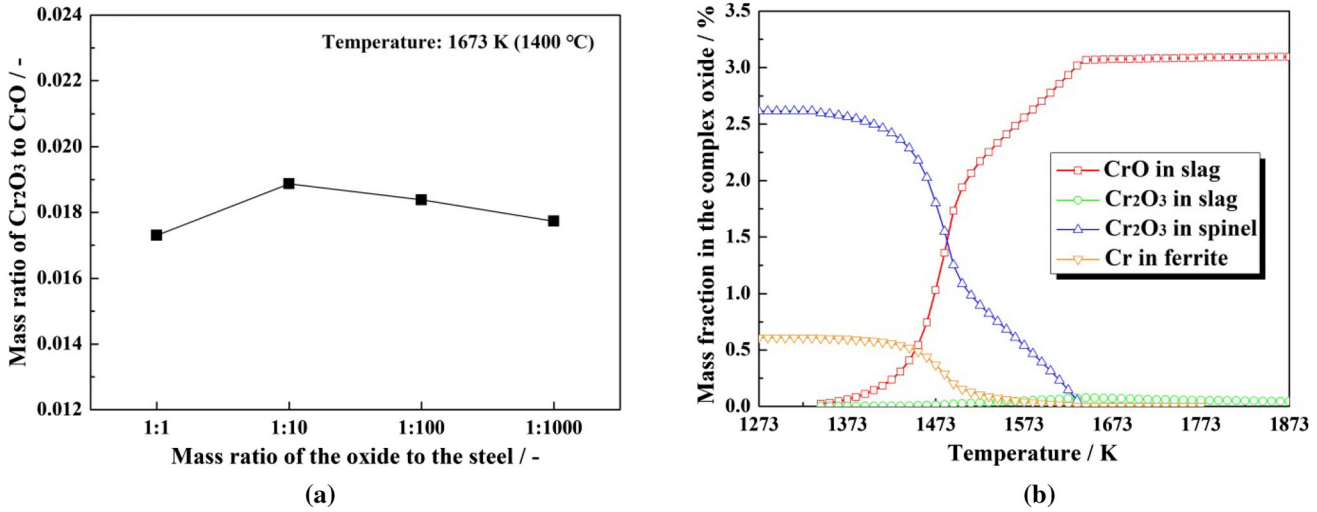


Fig. 11—(a) Relationship between the mass ratio of Cr_2O_3 to CrO in the equalized complex oxide B and the mass ratio of the oxide to the steel at 1673 K (1400 °C) and (b) transformation of Cr-containing phases inside the complex oxide at various isothermal heating temperatures.

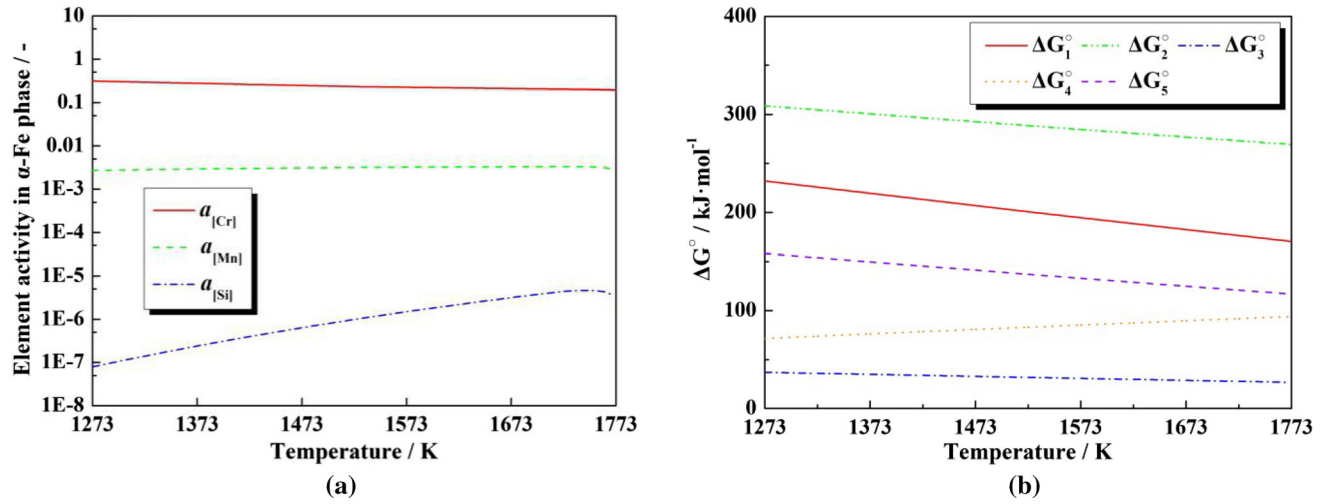
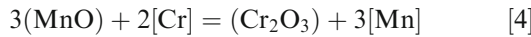
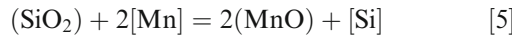


Fig. 12—Summary of thermodynamic data used for computing the Gibbs free energy changes of Eqs. [1] to [5] after isothermal heating: (a) activities of Cr, Mn and Si in α -Fe phase and (b) Standard Gibbs-free energy ΔG° for Eqs. [1] to [5].

$$J_3 = \frac{a_{(CrO)}a_{[Si]}}{a_{[Cr]}a_{(MnO)}}$$



$$J_4 = \frac{a_{(Cr_2O_3)}a_{[Mn]}^3}{a_{[Cr]}^2a_{(MnO)}^3}$$



$$J_5 = \frac{a_{(MnO)}^2a_{[Si]}}{a_{(SiO_2)}a_{[Mn]}^2}$$

where, J is the reaction quotient, $a_{(M_xO_y)}$ and $a_{[M]}$ are the activity of oxide component M_xO_y in the complex oxide and dissolved element M in the steel.

Thermodynamic equilibrium between the type 430 stainless steel and the complex MgO – Al_2O_3 – SiO_2 – CaO – MnO oxide at the interface was evaluated according to the Gibbs free energy changes of Eqs. [1] to [5] after isothermal heating. Activities of Cr, Mn, and Si in the steel and ΔG° of Eqs. [1] to [5] at the temperature range of 1273 to 1773 K (1000 to 1500 °C) were calculated and obtained by the Equilib module of FactSage 8.1 using the α -Fe phase and liquid slag phase as the standard states, and are shown in Figure 12. By combining simple oxides in the Eqs. [1] to [5], the formations of composite oxides have also been taken into consideration in the thermodynamic equilibrium calculations between the steel and the complex oxide. Thus, calculation results in the Figure 12 could be

directly employed to subsequently compute the Gibbs free energy changes of Eqs. [1] to [5] after isothermal heating.

Figures 7(c) and 8(c) show that, after isothermal heating at 1673 K (1400 °C) for 240 min, in all cases, the Si content in the steel decreased sharply within 50 μm distance from the interface. It was probably caused by the chemical equilibrium shift during the cooling process after heating. Here, taking the diffusion couple B-1400 as an example, the activities of Cr, Mn and Si in the temperature range of 1373 to 1673 K (1100 to 1400 °C) were calculated as a function of Si content in the steel. On the other hand, the activities of CrO, MnO and SiO_2 in the complex oxide were estimated using the average oxide composition in the diffusion couple B-1400 after isothermal heating at 1673 K (1400 °C) for 240 min. Since the chromium oxide was mainly CrO at 1673 K (1400 °C), the Gibbs free energy changes of Eqs. [1] and [5] as a function of Si content in the steel in the temperature range of 1373 to 1673 K (1100 to 1400 °C) were obtained, and are shown in Figures 13(a) and (b), respectively. Results indicated that with the temperature decreased from 1673 to 1373 K (1400 to 1100 °C), the predicted equalized Si content in the steel decreased significantly which was in agreement with experimental results.

Table I lists the initial chemical compositions of steel used for computing the Gibbs-free energy changes of Eqs. [1] to [5] before isothermal heating. Because the initial oxide contained no chromium oxide, the average oxide compositions after bonding were used as the initial oxide composition. The initial activities and Gibbs-free energy changes were obtained at the bonding temperature. After heating at 1673 K (1400 °C) for 240 min, since there was no concentration gradient in all oxides near the steel–slag interface, the bulk oxide composition was assumed as the one at the interface. Based on the analysis above, to avoid the influence of the cooling process after isothermal heating, the region in which the Si content in the steel near the steel–slag interface

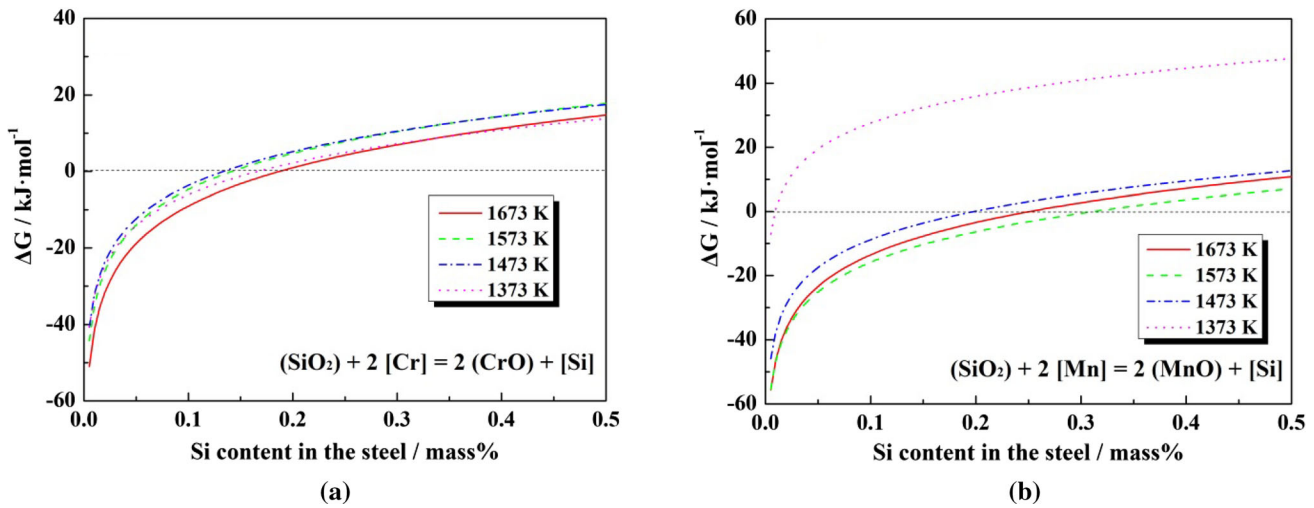


Fig. 13—Gibbs-free energy changes as a function of Si content in the steel in the temperature range of 1373 to 1673 K (1100 to 1400 °C) for the reactions: (a) $(\text{SiO}_2) + 2 [\text{Cr}] = 2 (\text{CrO}) + 1.5 [\text{Si}]$, and (b) $(\text{SiO}_2) + 2 [\text{Mn}] = 2 (\text{MnO}) + [\text{Si}]$.

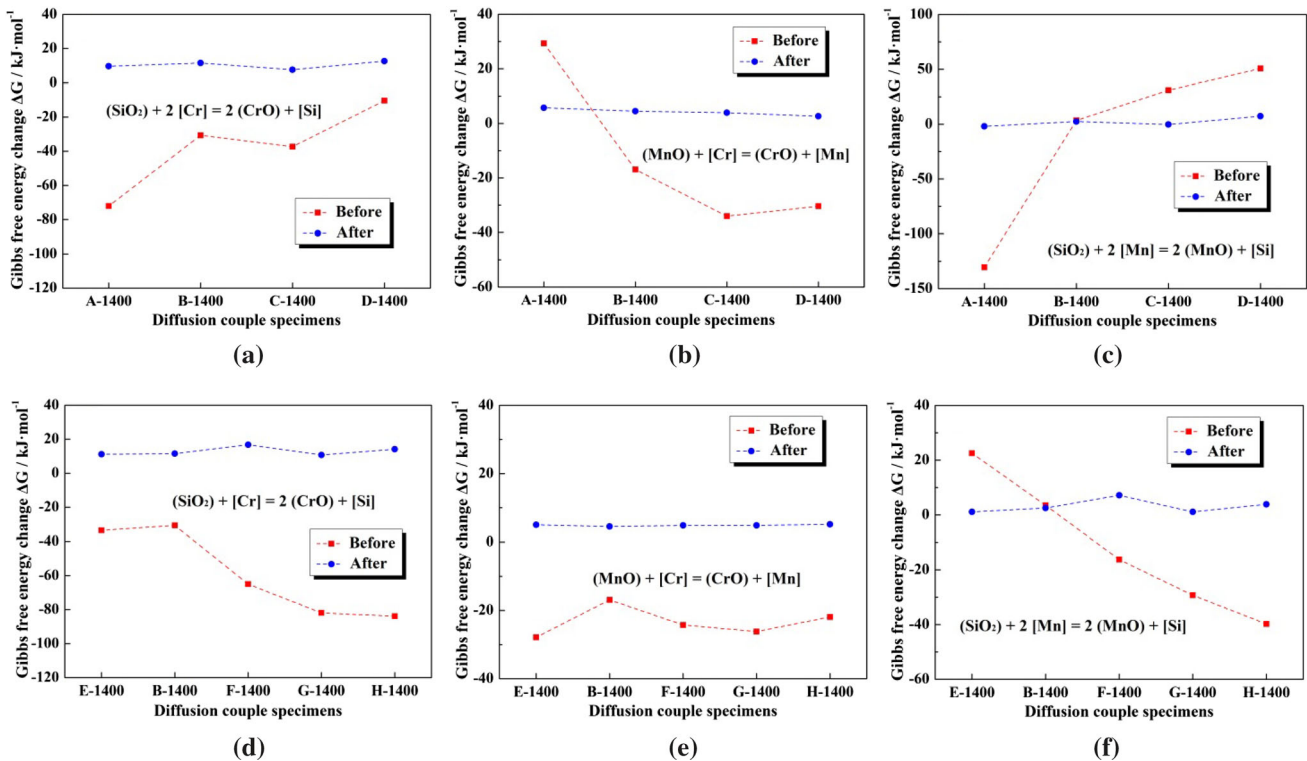


Fig. 14—Gibbs-free energy changes (ΔG) of Eqs. [1], [3] and [5] at the steel-oxide interfaces of different diffusion couple specimens before and after the isothermal heating at 1673 K (1400 °C) for 240 min: (a) Eq. [1] at the interface of diffusion couples A, B, C, and D; (b) Eq. [3] at the interface of diffusion couples A, B, C, and D; (c) Eq. [5] at the interface of diffusion couples A, B, C, and D; (d) Eq. [1] at the interface of diffusion couples E, B, F, G, and H; (e) Eq. [3] at the interface of diffusion couples E, B, F, G, and H; (f) Eq. [5] at the interface of diffusion couples E, B, F, G, and H.

showed a sharp decrease trend was excluded. The average steel composition measured at a distance of 50 to 100 μm from the interface was assumed to be the one at the interface after the heating. After heating at 1373 K (1100 °C) for 240 min, the average composition of the steel and oxide measured at a distance of 2 to 10 μm from the interface was assumed to be the corresponding ones at the interface.

Figure 14 shows the Gibbs free energy changes of Eqs. [1], [3] and [5] at the steel-oxide interfaces of different diffusion couple specimens before and after isothermal heating at 1673 K (1400 °C) for 240 min. Before heating, all diffusion couples were in the state of non-equilibrium. After heating at 1673 K (1400 °C), the “solid-liquid” steel-oxide reactions occurred and the ΔG values for Eqs. [1], [3] and [5] in all diffusion couples

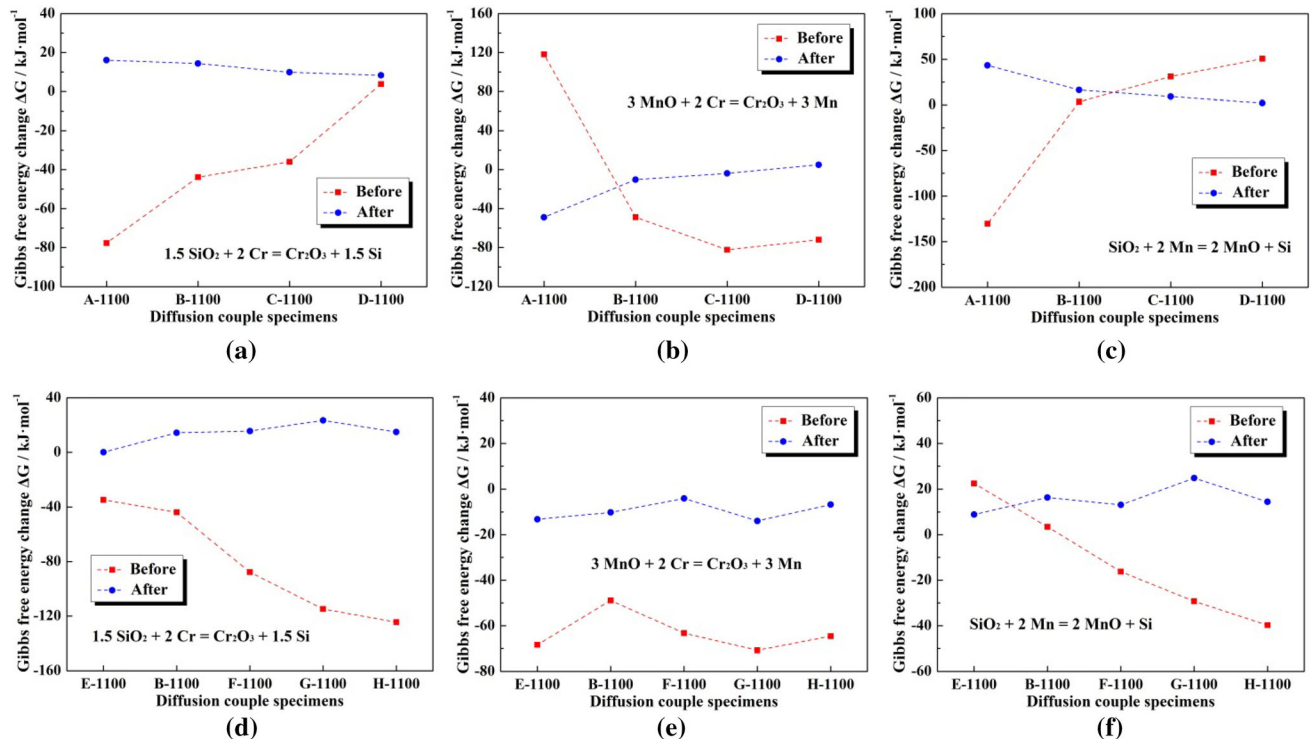


Fig. 15—Gibbs-free energy changes (ΔG) of Eqs. [2], [4] and [5] at the steel–oxide interface of different diffusion couple specimens before and after isothermal heating at 1373 K (1100 °C) for 240 min: (a) Eq. [2] at the interfaces of diffusion couples A, B, C, and D; (b) Eq. [4] at the interfaces of diffusion couples A, B, C, and D; (c) Eq. [5] at the interfaces of diffusion couples A, B, C, and D; (d) Eq. [2] at the interfaces of diffusion couples E, B, F, G, and H; (e) Eq. [4] at the interfaces of diffusion couples E, B, F, G, and H; (f) Eq. [5] at the interfaces of diffusion couples E, B, F, G, and H.

were close to 0, which indicated that thermodynamic equilibrium between the steel and oxide was achieved. Experimental results after isothermal heating at 1673 K (1400 °C) were all in agreement with the thermodynamic evaluation by the calculation of Gibbs-free energy changes.

Figure 15 shows the Gibbs-free energy changes of Eqs. [2], [4] and [5] at the steel–oxide interface of different diffusion couple specimens before and after isothermal heating at 1373 K (1100 °C) for 240 min. Before heating, all diffusion couples were also in the state of non-equilibrium. After heating at 1373 K (1100 °C), the “solid–solid” steel–oxide reactions occurred and the ΔG values at the steel–oxide interface for Eqs. [2], [4] and [5] in all diffusion couples tended to be 0. The initial MnO and SiO₂ contents in the complex oxides only affected the original Gibbs free energy changes before isothermal heating. However, after heating at 1373 K (1100 °C) for 240 min, the thermodynamic equilibrium between the steel and oxide at the interface in all diffusion couples were generally achieved except the diffusion couple A-1100. Since the initial oxide A contained no MnO, the thermodynamic equilibrium seemed more difficult to achieve. Forward or backward reactions of Eqs. [2], [4] and [5] occurred at the steel–oxide interface during heating and caused variations of Cr, Mn and Si contents in the steel and Cr₂O₃, MnO and SiO₂ in the complex oxide.

Table VI. Calculated Diffusion Coefficients of Cr, Mn and Si in Steel at 1673 K (1400 °C)

Specimen	$D_{Cr}/m^2 s^{-1}$	$D_{Mn}/m^2 s^{-1}$	$D_{Si}/m^2 s^{-1}$
A-1400	2.58×10^{-12}	0.68×10^{-11}	0.80×10^{-11}
B-1400	1.68×10^{-12}	—	—
C-1400	3.33×10^{-12}	1.19×10^{-11}	0.56×10^{-11}
D-1400	3.40×10^{-12}	0.99×10^{-11}	1.34×10^{-11}
E-1400	1.44×10^{-12}	—	0.52×10^{-11}
F-1400	1.84×10^{-12}	—	1.03×10^{-11}
G-1400	3.14×10^{-12}	1.01×10^{-11}	0.70×10^{-11}
H-1400	2.89×10^{-12}	0.42×10^{-11}	1.26×10^{-11}

Table VII. Calculated Diffusion Coefficients of Mn and Si in Steel at 1373 K (1100 °C)

Specimens	$D_{Mn}/m^2 s^{-1}$	$D_{Si}/m^2 s^{-1}$
A-1100	3.71×10^{-13}	5.64×10^{-13}
B-1100	0.92×10^{-13}	4.95×10^{-13}
C-1100	1.31×10^{-13}	—
D-1100	0.80×10^{-13}	1.19×10^{-13}
E-1100	1.06×10^{-13}	—
F-1100	0.97×10^{-13}	1.04×10^{-13}
G-1100	0.99×10^{-13}	—
H-1100	—	1.43×10^{-13}

B. Kinetic Analysis of the Interfacial Reaction

During isothermal heating at 1673 and 1373 K (1400 and 1100 °C), respectively, “solid–liquid” and “solid–solid” steel–oxide interfacial reactions occurred between Cr, Mn and Si in the steel and CrO_x, MnO and SiO₂ in the oxide, resulting in the concentration gradient of Cr, Mn and Si in steel. When two semi-infinite bars differing in composition were joined at the plane $x = 0$ to form a diffusion couple, the distribution of diffusion elements were subject to Eq. [6].^[25]

$$C_i(x, t) = C_i(\text{Matrix}) + [C_i(\text{Interface}, t) - C_i(\text{Matrix})] \times \left(1 - \operatorname{erf}\left(\frac{x}{2\sqrt{D_i t}}\right) \right) \quad [6]$$

where x is the distance from the steel–oxide interface, t is the isothermal heating time, D_i is the diffusion coefficient of element i , $C_i(\text{Matrix})$ is the initial concentration of element i in steel matrix, $C_i(\text{Interface}, t)$ and $C_i(x, t)$ are the concentrations of element i at the interface and position x at time t , respectively. Thus, using the steel composition measured by EPMA in Figures 7 through 10, the diffusion coefficients of Cr, Mn and Si during heating were calculated.

For the diffusion couples heat treated at 1673 K (1400 °C), the initial concentration of element i in steel matrix, $C_i(\text{Matrix})$, was obtained from Table I. Since the final concentration of steel at the interface was affected by the chemical equilibrium shift during the cooling process after heating, the equalized concentrations of elements at the interface, $C_i(\text{Interface}, t)$, were predicted using fitting curves which were plotted using the steel composition measured within a distance of 100 to 400 μm from the interface. The $C_i(x, t)$ at different distance from the steel–oxide interface ($x = 150, 200, 250, 300$ and $350 \mu\text{m}$) was obtained to calculate corresponding diffusion coefficient of element i . An average value of those diffusion coefficients of element i at different distances was obtained. For the diffusion couples heat treated at 1373 K (1100 °C), similarly the initial concentration of element i in steel matrix, $C_i(\text{Matrix})$, was obtained from Table I. Fitting curves were also plotted using the steel composition measured with a distance of 2 to 150 μm from the interface. The concentrations of element i at the interface ($x = 0$), $C_i(\text{Interface}, t)$, and $C_i(x, t)$ at different distance from the steel–oxide interface ($x = 25, 50, 75, 100$ and $125 \mu\text{m}$) were obtained to calculate corresponding diffusion coefficient of element i . Then, an average value of those diffusion coefficients of element i at different distances was also achieved.

In some diffusion couples, the diffusion coefficients of Mn and Si could not be obtained because there were no concentration gradients after heating. Table VI shows the calculated diffusion coefficients of Cr, Mn, and Si in different diffusion couples at 1673 K (1400 °C), which are in the range of 1.44 to 3.40×10^{-12} , 0.42 to 1.19×10^{-11} and 0.52 to $1.34 \times 10^{-11} \text{ m}^2 \text{ s}^{-1}$, respectively.

Figures 9 and 10 show that there was obvious phase separation in the steel matrix after isothermal heating at 1373 K (1100 °C) and it led to the fluctuation of Cr content in the steel. Since it was difficult to distinguish the Cr diffusion to the steel–oxide interface and to the Cr-riched phases in the steel during heating, only the diffusion coefficients of Mn and Si were evaluated for isothermal heating at 1373 K (1100 °C), as listed in Table VII, where the diffusion coefficients of Mn and Si are in the range of 0.80 to 3.71×10^{-13} and 1.04 to $5.64 \times 10^{-13} \text{ m}^2 \text{ s}^{-1}$, respectively. Generally, the diffusion coefficients in the steel at 1373 K (1100 °C) were relatively lower than those at 1673 K (1400 °C), which were in good agreement with the phenomena observed in the heating experiments.

As indicated by Eqs. [1] through [5] in the thermodynamic analysis, the “solid–liquid” and “solid–solid” steel–oxide interface reactions during isothermal heating at 1673 K and 1373 K (1400 °C and 1100 °C) were generally controlled by diffusion of Cr, Mn and Si to the oxides or away from the oxides, depending on the initial MnO and SiO₂ content in the oxide. A higher temperature improves the diffusion of elements such as [Mn], [Cr] and [Si] in the steel, resulting in the variation of MnO, CrO_x and SiO₂ content in the oxide to reach equilibrium. Determination of the diffusion coefficients of [Mn], [Cr] and [Si] in the steel contributes to precisely predicting and controlling the transformation of complex inclusions during isothermal heating before hot rolling processes, which is also essential for improving mechanical properties of type 430 stainless steel.

V. CONCLUSIONS

In the present study, diffusion couple experiments at 1373 K and 1673 K (1100 °C and 1400 °C) between type 430 stainless steel and complex MgO–Al₂O₃–SiO₂–CaO–MnO oxide with different MnO and SiO₂ contents were conducted to quantitatively study the mechanism of “solid–liquid” and “solid–solid” steel–oxide interface reactions during the soaking process before hot-rolling. The conclusions are as follows:

1. The “solid–liquid” and “solid–solid” steel–oxide reactions occurred between Cr, Mn and Si in the steel and MnO and SiO₂ in the MgO–Al₂O₃–SiO₂–CaO–MnO oxide during heating at 1373 K and 1673 K (1100 °C and 1400 °C), respectively, due to their non-equilibrium states, and resulted in the change of steel and oxide compositions.
2. The Gibbs free energy changes of those steel–oxide reactions before and after isothermal heating indicated thermodynamic equilibrium at the interface of the steel and oxide were generally achieved after the isothermal heating at 1373 K and 1673 K (1100 °C and 1400 °C) for 240 min.
3. Diffusion coefficients of related elements in type 430 stainless steel at 1373 K and 1673 K (1100 °C and 1400 °C) were obtained: Cr, Mn, and Si at 1673 K

(1400 °C) are in the range of 1.44 to 3.40×10^{-12} , 0.42 to 1.19×10^{-11} and 0.52 to $1.34 \times 10^{-11} \text{ m}^2 \text{ s}^{-1}$, respectively, while Mn and Si at 1373 K (1100 °C) are in the range of 0.80 to 3.71×10^{-13} and 1.04 to $5.64 \times 10^{-13} \text{ m}^2 \text{ s}^{-1}$.

ACKNOWLEDGMENTS

The current study was supported by the National Natural Science Foundation of China (Grant Nos. 52074198, 51774217 and 51604201).

CONFLICT OF INTEREST

On behalf of all authors, the corresponding author states that there is no conflict of interest.

REFERENCES

1. S.K. Gupta, A.R. Raja, M. Vashista, and M.Z.K. Yusufzai: *Mater. Res. Express.*, 2018, vol. 6, art. no. 036516.
2. L.L. Wei, J.H. Zheng, L.H. Chen, and R.D.K. Misra: *Corros. Sci.*, 2018, vol. 142, pp. 79–92.
3. L. Tanure, C.M.D. Alcântarac, D.B. Santos, T.R.D. Oliveirac, B.M. Gonzalez, and K. Verbeken: *J. Mater. Res. Technol.*, 2019, vol. 8, pp. 4048–65.
4. T.L. Liu, X.F. Zhu, L.J. Chen, H.Y. Bi, Y.F. Lin, and J. Long: *J. Mater. Sci.*, 2019, vol. 55, pp. 3584–99.
5. Y. Han, J.Q. Sun, Y. Sun, J.P. Sun, and X. Ran: *Metals*, 2020, vol. 10, art. no. 86.
6. K.A. Cashell and N.R. Baddoo: *Thin. Wall. Struct.*, 2014, vol. 83, pp. 169–81.
7. H.J. Bong and J. Lee: *Int. J. Mech. Sci.*, 2021, vol. 191, art. no. 106066.
8. X.R. Guan, D.L. Zhang, and Y.H. Jin: *Appl. Mech. Mater.*, 2014, vol. 6, pp. 651–53.
9. F. Shang, X.Q. Chen, P. Zhang, F. Ming, Z.C. Ji, S.B. Ren, and X.H. Qu: *Mater. Trans.*, 2019, vol. 60, pp. 1096–1102.
10. G. Okuyama, K. Yamaguchi, S. Takeuchi, and K.I. Sorimachi: *ISIJ Int.*, 2000, vol. 40, pp. 121–28.
11. W.Y. Cha, D.S. Kim, Y.D. Lee, and J.J. Pak: *ISIJ Int.*, 2004, vol. 44, pp. 1134–39.
12. J.H. Park, D.S. Kim, and S.B. Lee: *Metall. Mater. Trans. B*, 2005, vol. 36B, pp. 67–73.
13. J.H. Park and D.S. Kim: *Metall. Mater. Trans. B*, 2005, vol. 36B, pp. 495–502.
14. J.H. Park: *Calphad*, 2011, vol. 35, pp. 455–62.
15. Z.H. Jiang, S.J. Li, and Y. Li: *J. Iron Steel Res. Int.*, 2011, vol. 18, pp. 14–17.
16. X. Yin, Y. Sun, Y. Yang, X. Deng, M. Barati, and A. McLean: *Ironmak. Steelmak.*, 2016, vol. 44, pp. 152–58.
17. Y. Wang, M.K. Oh, T.S. Kim, A. Karasev, W.Z. Mu, J.H. Park, and P.G. Jönsson: *Metall. Mater. Trans. B*, 2021, vol. 52B, pp. 3815–32.
18. C. Gu, M. Wang, Y.P. Bao, F.M. Wang, and J.H. Lian: *Metals*, 2019, vol. 9, pp. 476–91.
19. Q. Wang, X.D. Zou, H. Matsuura, and C. Wang: *Metall. Mater. Trans. B*, 2017, vol. 49B, pp. 18–22.
20. Y.K. Yang, D.P. Zhan, H. Lei, Y.L. Li, X. Liu, Z.H. Jiang, and H.S. Zhang: *Metall. Mater. Trans. B*, 2021, vol. 52B, pp. 1839–53.
21. A.I. Zaitsev, A.V. Koldaev, A.V. Amezhnov, and N.G. Shaposhnikov: *Metallurgist*, 2016, vol. 60, pp. 1–9.
22. Y.X. Zhang, L.F. Zhang, Y.P. Chu, Q. Ren, J.J. Wang, N. Liu, Z.Y. Chen, and J.G. Zhi: *Steel Res. Int.*, 2020, vol. 91, art. no. 2000120.
23. J. Guo, X.R. Chen, S.W. Han, Y. Yan, and H.J. Guo: *Int. J. Min. Met. Mater.*, 2020, vol. 27, pp. 328–39.
24. W.L. Gan, C.S. Liu, K. Liao, H. Zhang, and H.W. Ni: *Metall. Mater. Trans. B*, 2022, vol. 53B, pp. 485–502.
25. H. Mehrer: *Diffusion in Solids: Fundamentals, Methods, Materials, Diffusion-Controlled Processes*, Springer, Berlin, 2007.

Publisher's Note Springer Nature remains neutral with regard to jurisdictional claims in published maps and institutional affiliations.